Supplemental material to the article: Reduced order modeling of combustion instabilities in liquid rocket engines

M. Gonzalez-Flesca*, P. Scouflaire†, T. Schmitt‡, S. Ducruix§, and S. Candel¶
Laboratoire EM2C, CNRS, CentraleSupélec, Université Paris-Saclay
3 rue Joliot Curie, Bat. Eiffel, 91192 Gif-sur-Yvette cedex, France

Y. Méry‖
SAFRAN Aircraft Engines
77550 Moissy-Cramayel, France

*PhD, Ingénieur ISAE-ENSMA, m.gonzalezflesca@gmail.com
†Ingénieur de recherche au CNRS, philippe.scouflaire@centralesupelec.fr
‡Chargé de recherche au CNRS, thomas.schmitt@centralesupelec.fr
§Directeur de recherche au CNRS, sebastien.ducruix@centralesupelec.fr
¶Professeur des Universités, sebastien.candel@centralesupelec.fr
‖Expert engineer at Safran Aircraft Engines,yoann.mery@safrangroup.com

A. A brief review of eigenmodes and eigenfrequencies

The previous framework relies on a modal expansion of the pressure field. Let us then start examining these normal modes and the corresponding eigenfrequencies. Normal modes are solutions of a Helmholtz equation ([1]).

$$\nabla^2 \Psi_n + \frac{\omega_n^2}{c^2} \Psi_n = 0 \tag{1}$$

In general, the walls of the system are rigid with the exception of inlets and outlets. The boundary conditions that describe this situation can be written as

$$\boldsymbol{n} \cdot \nabla \Psi_n = 0 \tag{2}$$

Solutions of the previous boundary value problem are easily determined for simple geometries. This is exemplified in what follows for rectangular and cylindrical cavities.

1. Rectangular geometry

This case is examined here because it is the simplest and also because it corresponds to the geometry of the cavities of the NPCC test rig, which is presented in the next section. For rectangular cavities and rectangular geometries in general, the pressure field p must satisfy the Helmholtz equation. The solution of the boundary value problem defined by the Helmholtz equation and rigid wall boundary conditions may be obtained by writing Ψ in the form of a product $\Psi(x, y, z) = X(x)Y(y)Z(z)$. The Helmholtz equation becomes

$$\frac{X''}{X} + \frac{Y''}{Y} + \frac{Z''}{Z} + k^2 = 0 \tag{3}$$

where $k = \omega/c$. The first three terms in the previous expression depend on a the three spatial variables. One may then deduce that each of these terms must be constant. It is convenient to designate the respective constants by κ_x^2, κ_y^2 and κ_z^2. These quantities must satisfy the condition $k^2 = \kappa_x^2 + \kappa_y^2 + \kappa_z^2$. The three functions X, Y and Z have to satisfy $X'' + \kappa_x^2 X = 0$, $Y'' + \kappa_y^2 Y = 0$ and $Z'' + \kappa_z^2 Z = 0$. These three equations with the zero normal velocity boundary conditions yield the following eigenfunctions

$$X = \cos(\kappa_x x) \quad Y = \cos(\kappa_y y) \quad Z = \cos(\kappa_z z) \tag{4}$$

with the following values for the wave numbers

$$\kappa_x = \frac{n_x \pi}{l_x} \quad \kappa_y = \frac{n_y \pi}{l_y} \quad \kappa_z = \frac{n_z \pi}{l_z} \tag{5}$$

where (n_x,n_y,n_z) is an integer triplet. The pressure field in the domain is then given by equation 6.

$$\Psi_{n_x,n_y,n_z} = \cos\left(\frac{n_x\pi x}{l_x}\right)\cos\left(\frac{n_y\pi y}{l_y}\right)\cos\left(\frac{n_z\pi z}{l_z}\right) \tag{6}$$

The corresponding angular frequency ω can be deduced from

$$k^2 = \pi^2\left[\left(\frac{n_x}{l_x}\right)^2 + \left(\frac{n_y}{l_y}\right)^2 + \left(\frac{n_z}{l_z}\right)^2\right]$$

and the eigenfrequency corresponding to the mode (n_x,n_y,n_z) is given by

$$f = \frac{c_0}{2}\left[\left(\frac{n_x}{l_x}\right)^2 + \left(\frac{n_y}{l_y}\right)^2 + \left(\frac{n_z}{l_z}\right)^2\right]^{\frac{1}{2}} \tag{7}$$

2. Cylindrical chamber geometry

We now consider a cylindrical domain of radius R and length L. The analysis closely follows that used in the case of a rectangular geometry. It is natural to use cylindrical coordinate system (r,θ,x) and write the Helmholtz equation in the form

$$\frac{\partial^2\Psi}{\partial r^2} + \frac{1}{r}\frac{\partial\Psi}{\partial r} + \frac{1}{r^2}\frac{\partial^2\Psi}{\partial\theta^2} + \frac{\partial^2\Psi}{\partial x^2} + \frac{\omega^2}{c^2}\Psi = 0 \tag{8}$$

One finds after some calculations that the modes are determined by three integers m,n and q corresponding to the radial, azimuthal and longitudinal directions respectively. The eigenmodes are given by the following expression:

$$\Psi_{m,n,q}(r,\theta,x) = J_n\left(\frac{\pi\beta_{mn}r}{R}\right)\cos\left(\frac{q\pi x}{L}\right)\left(ae^{in\theta} + be^{-in\theta}\right) \tag{9}$$

where a and b are two complex amplitudes, J_n is the Bessel function of order n of the first kind, and β_{mn} are the roots of $J_n'(\pi\beta_{mn}) = 0$. The resonant frequencies are then given by

$$f_{mnq} = \frac{c}{2}\left[\left(\frac{\beta_{mn}}{R}\right)^2 + \left(\frac{q}{L}\right)^2\right]^{\frac{1}{2}} \tag{10}$$

It is worth noting that the modes defined by expression (9) are degenerate. There is an infinity of modal structures corresponding to each of the eigenfrequencies defined by expression (10). The corresponding structures are defined by the possible combinations of the complex amplitudes a and b. For example if $b = 0$ and $a \neq 0$, the mode has an azimuthal structure that behaves like $e^{in\theta - i\omega t}$. This is a wave rotating in the positive θ direction (i.e. the counterclockwise direction). If $a = 0$ and $b \neq 0$ the azimuthal structure behaves like $e^{-in\theta - i\omega t}$. This wave rotates in the negative θ

direction (i.e. the clockwise direction). If $a = b$, the two complex exponentials combine to form a cosine structure: $\cos(n\theta)e^{-i\omega t}$. This forms a standing mode with a nodal line at $\theta = \pi/2$. The position of the pressure nodal and anti-nodal lines do not change with time.

B. The Very High Amplitude Modulator of the NPCC test rig

(a) 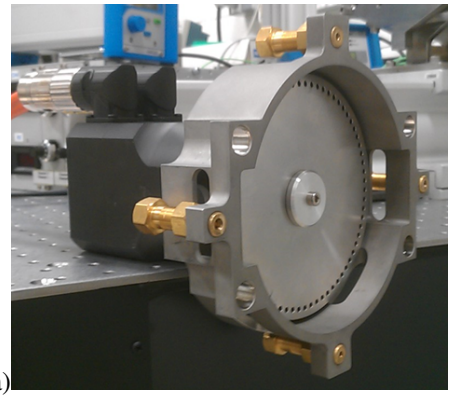 (b) 

Fig. 1 (a) Photograph of the fully perforated wheel mounted on the electric motor of the VHAM. (b) Photograph of the half perforated wheel used to study damping in the system.

C. Eigenmodes and eigenfrequencies of the NPCC test rig

The eigenmodes of the system are important because they define the resonant frequencies at which the system responds with the greatest intensity. For a single box-like cavity with rigid walls, equation 7 is sufficient to determine the eigenmodes. However, for coupled cavities the situation is much more complicated. The ramp mode of operation of the motor is well suited for the determination of the eigenmodes of the domain. The frequency of modulation is slowly increased from 0 Hz to 3000 Hz during a ramp of 99 s. As an illustration, pressure oscillations are observed at positions HFc1 and HFd1. The recordings presented in figure 2(a) show a strong pressure response at few intervals during the experiment. It is then possible to determine the times of maximum response and obtain the corresponding frequencies, which characterize the different eigenmodes. The time-frequency analysis shown in figure 2(b) also provides the eigenfrequencies of the system.

The numerical determination of eigenmodes can be carried out by a general purpose Helmholtz solver such as AVSP, developed by CERFACS and used in the prensent work. An overview of the code is given in [2, 3]. This three dimensional acoustic solver is more flexible than the analytical method described previously and it can be used in the design process to determine the modal structures and resonant frequencies more precisely. It is also possible to impose more complex impedance boundary conditions rather than the zero normal velocity at the boundary. AVSP can also be used to deal with a non-uniform temperature field. Here the results of the ramp test will be compared with results provided by the numerical Helmholtz solver in which all boundary conditions were null velocity boundaries. The results

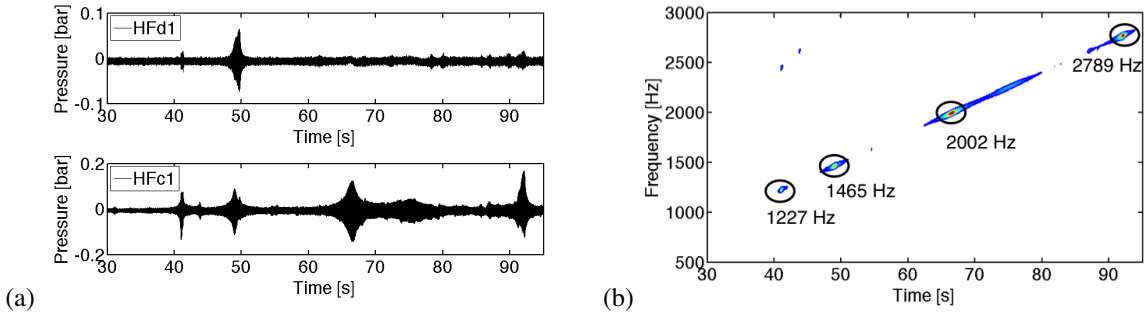

Fig. 2 (a) Pressure signal recorded at positions HFc1 and HFd1 as a function of time during a ramp test. Each peak corresponds to an eigenmode in the cavity. (b) Short time Fourier transform analysis of the signal detected at HFc1. The circled area represents eigenfrequencies of the domain.

of the AVSP simulation are displayed in figure 3. The 1T1L mode of the chamber does correspond to a 1T mode in the dome.

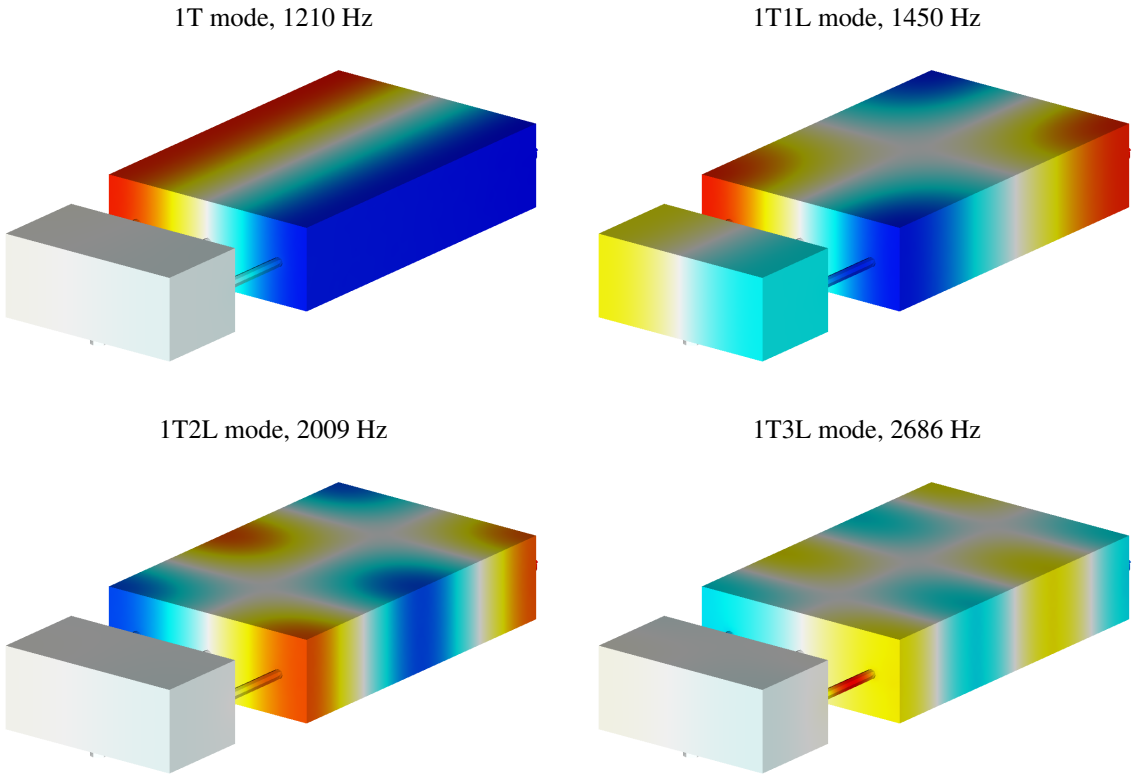

Fig. 3 A selected set of eigenmodes of the NPCC configuration, as found by the AVSP solver.

D. Damping determination methodology

In order to study the acoustic damping, a half perforated wheel (figure 1(b)) was used. This wheel allows the generation of acoustic modes in the domain when the perforations pass in front of the nozzles. A sudden interruption of

the modulation occurs when the smooth part of the wheel passes in front of the nozzles, this allows the system to relax. The design of the wheel makes it possible to evacuate the air at a constant flow rate. In addition, as already exposed, in order to generate various pressure losses in the three injectors, head loss diaphragms can be accommodated in the injector plate.

The system can be described as a second order oscillator. When the perforations modulate the nozzles, the system is driven and the amplitude increases up to a certain level. This happens during the first half of a wheel rotation. During the second half, the two nozzles are half open and there is no modulation. During that period, the dynamics is that of a second order system with no forcing:

$$\ddot{\eta}(t) + 2\alpha\dot{\eta}(t) + \omega^2\eta(t) = 0 \tag{11}$$

where η is the amplitude of the pressure fluctuation based on modal projection, α is the damping rate and ω is the angular frequency corresponding to one of the eigenmodes of interest. The analytical solution of the differential equation 11 is given in equation 12:

$$\eta(t) = e^{-\alpha t}\left(a\exp[it(\omega^2 - \alpha^2)^{1/2}] + b\exp[-it(\omega^2 - \alpha^2)^{1/2}]\right) \tag{12}$$

where a and b are integration constants. The entire pressure amplitude is multiplied by $e^{-\alpha t}$ indicating that the pressure signal is bounded by an exponential function decreasing at a rate fixed by α that is the damping rate. The approach proposed here consists in determining the damping rate α by experimental means. Records of pressure detected by the acoustic sensors take the form of periodic oscillations containing two main parts: the generation of the acoustic modulation and the subsequent relaxation. The analysis of these recordings allow the determination of the damping rates. During the relaxation of the pressure oscillations the envelope of the signal is proportional to $e^{-\alpha t}$ (figure 4(a)). The damping rate is evaluated by taking the neperien logarithm of the envelope of the damped oscillation, plotting it as a function of time and reading the slope (figure 4(b)). This method will be referred to as the relaxation method.

E. Presentation of the BKD engine

The full-scale rocket engine proposed for this study is the BKD test rig operated at DLR Lampoldshausen Germany. This engine is interesting because, under certain conditions it becomes naturally unstable. The BKD test rig is a cylindrical combustion chamber featuring 42 coaxial injectors injecting liquid oxygen and hydrogen, operating in the transcritical regime. Figure 5 shows an illustration of the engine. More detailed information can be found in [4]. The chamber is instrumented with a ring of eight high frequency pressure sensors around the injector plate and in the dome. This arrangement allows a proper detection (frequency, amplitude) of high frequency spinning modes in the azimuthal

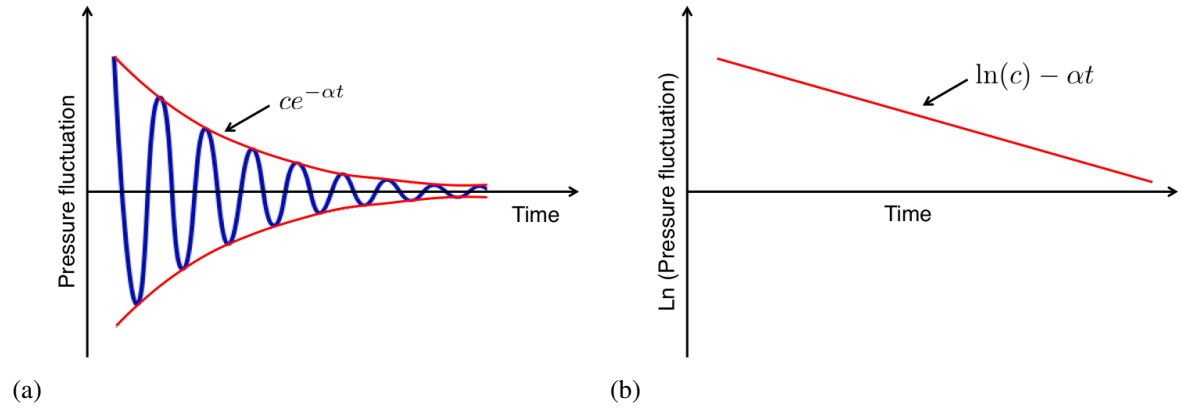

Fig. 4 (a) Schematic view of the damping of pressure oscillations. – (blue line) Pressure signal at HFc1, – (red line) envelope of the pressure signal at HFc1. (b) Schematic view of the logarithm of the envelope of the pressure signal.

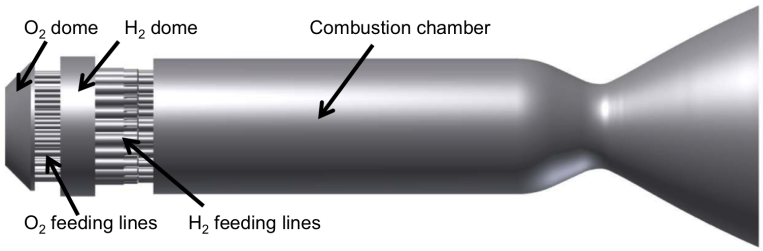

Fig. 5 Illustration of the BKD engine.

direction inside the chamber. The four Load Points (LP) studied at the DLR are summarized in table 1. The present simulations focus on LP3 and LP4, LP3 is found to be stable, while LP4 is unstable presenting large amplitude (around 2.0 MPa peak-to-peak) high frequency acoustic fluctuations. In addition, these two cases feature similar injection conditions (mass flow rate, oxygen temperature), except for the hydrogen temperature, which is lower for LP3 than for LP4. Under LP3 or LP4 injection conditions, the chamber pressure is around 8.0 MPa, while LP1 and LP2 have a chamber pressure around 7.0 MPa. Based on similarities of the operating conditions of LP3 and LP4, we made the assumption that the damping rates can be considered the same for these two cases. This assumption could not be made for any of the other operating conditions available since several damping mechanisms depend, among other things, on the injection conditions, the temperature in the cavities, the burnt gas composition, the turbulence.

F. Eigenmodes and eigenfrequencies of the BKD engine

A set of eigenfrequencies and modes for LP3 (the stable load point corresponding to injection of low temperature hydrogen) are displayed in figure 6 while the eigenfrequencies and modes for LP4 (the unstable load point corresponding to higher temperature hydrogen injection) are displayed in figure 7.

The AVSP code applied to the BKD under the conditions LP3 yields a large number of eigenmodes and

Case LP3

spinning 1A mode, 8167 Hz

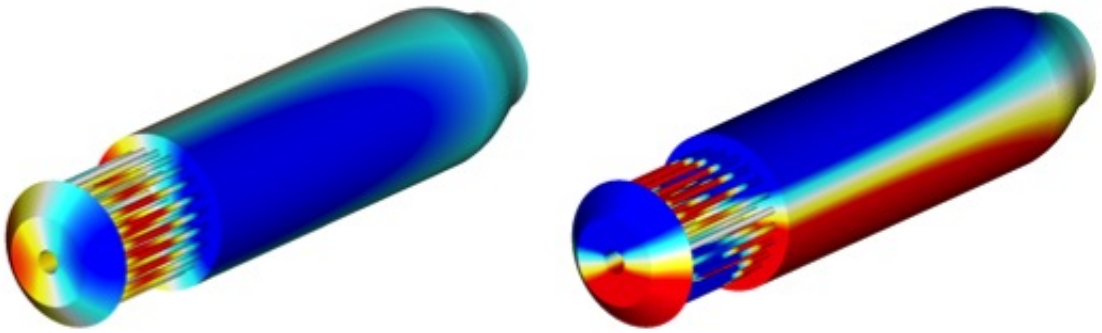

spinning 1A1L mode, 8606 Hz

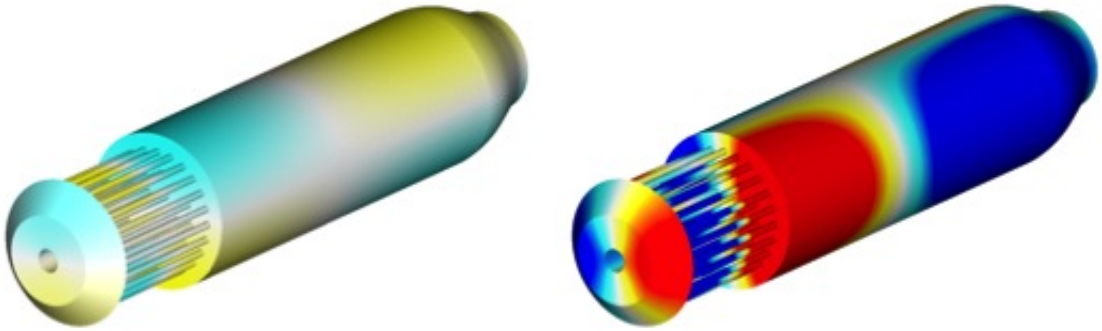

spinning 1A2L mode, 9482 Hz

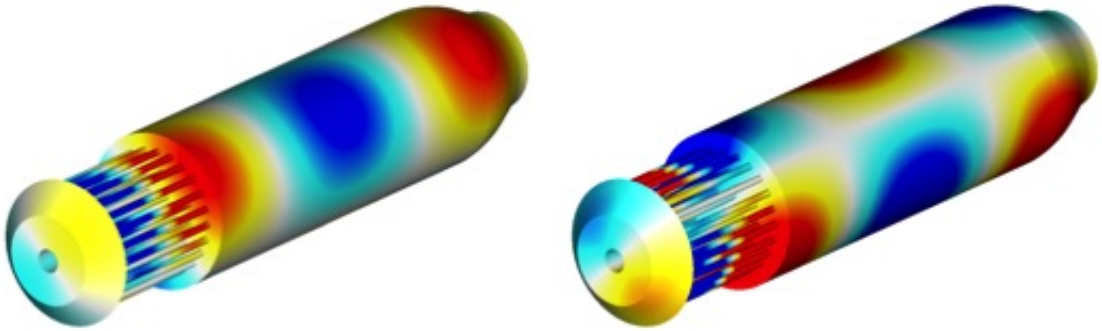

Fig. 6 Eigenmodes for case LP3.

Table 1 The four operating conditions studied at DLR. p^{dome} is the dome mean pressure, T^{dome} is the dome mean pressure, $\dot{m}_{LOx}$ and $\dot{m}_{H_2}$ are the mass flow rates of oxygen and hydrogen, respectively. MR is the mixture ratio defined by $MR = \dot{m}_{LOx}/\dot{m}_{H_2}$ and J the momentum flux ratio defined by $J = \rho^i_{H_2}(\overline{u}^i_{H_2})^2/\rho^i_{LO_2}(\overline{u}^i_{LO_2})^2$.

Load Point	LP1	LP2	LP3	LP4
$\dot{m}_{LOx}$ [kg.s^{-1}]	4.44	5.04	5.77	5.75
$\dot{m}_{H_2}$ [kg.s^{-1}]	1.11	0.84	0.96	0.96
$T^{dome}_{O_2}$[K]	126.46	126.21	123.06	126.16
$T^{dome}_{H_2}$[K]	111.80	112.77	79.74	113.38
$p^{dome}_{O_2}$[MPa]	7.841	8.111	9.189	9.410
$p^{dome}_{H_2}$[MPa]	10.003	8.966	9.012	10.292
MR	4	6	6.01	5.99
J	5.21	11.07	27.65	16.11

eigenfrequencies. Some of these frequencies correspond to purely longitudinal modes such as the 3L mode at 6565 Hz and others pertain to mixed modes like the spinning-longitudinal modes. It is interesting to note that the 1A, 1A1L and 1A2L are respectively found at frequencies of 8167 Hz, 8606 Hz and 9482 Hz (the "A" in the mode stands for azimuthal, the mode may be spinning or standing), the modal structure in the chamber is coupled with the modal structure inside the dome. In this cavity, for the three modes presented in figure 6, the azimuthal mode is weakly coupled to the chamber indicating that the maximum pressure in the dome faces a maximum of pressure in the chamber. This type of coupling will only create small pressure differences between the inlet and outlet of the various injectors and it is expected to induce weak mass flow rate fluctuations in the injection channels. In comparison with the frequencies for LP3, the frequencies for LP4 correspond to significantly higher values for the same modal structures (figure 7). The 3L mode is at 9991 Hz and the mixed modes 1A, 1A1L and 1A2L are at 10280 Hz, 10749 Hz and 11811 Hz, respectively. These frequencies are close to the frequencies of self-sustained instabilities found in the experimental work of the BKD ([5, 6]). As seen in ([6]), the different injection temperatures of hydrogen (table 1) have a strong impact in the frequencies of the eigenmodes of the system. Contrary to LP3, the maximum pressure in the dome faces a minimum of pressure in the chamber. One can notice from the analysis of figures 6 and 7 that each eigenmode is represented by two modal structures perpendicular to each other. This comes from the ASVP code, which projects the eigenmodes onto two perpendicular structures to indicate that the eigenmode found is a spinning mode.

Case LP4

spinning 1A mode, 10280 Hz

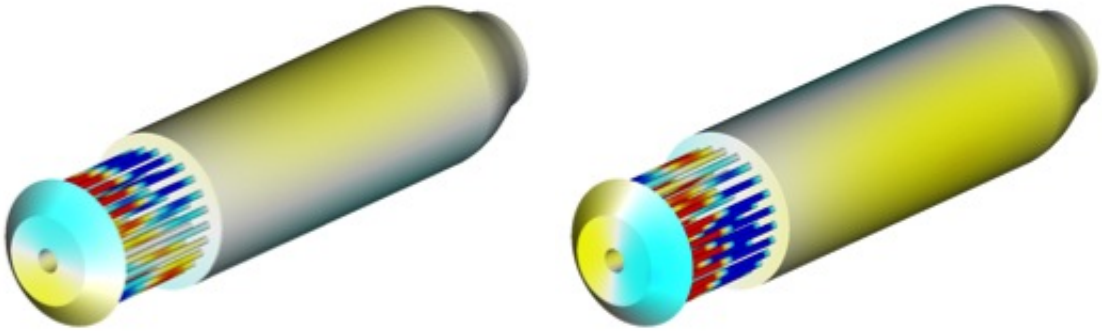

spinning 1A1L mode, 10749 Hz

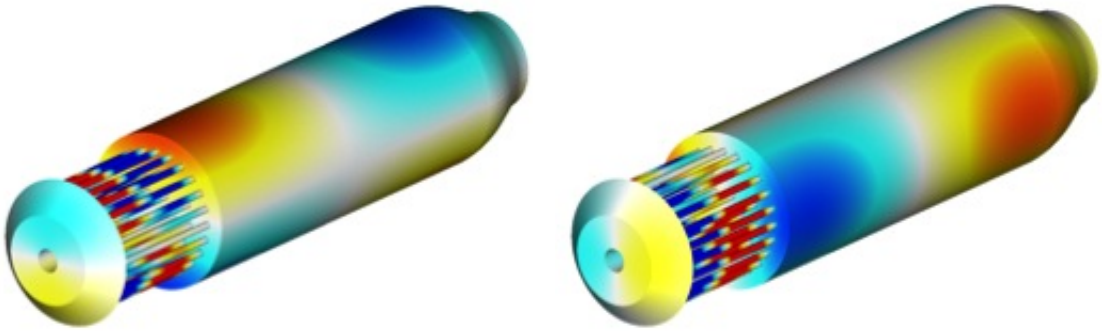

spinning 1A2L mode, 11811 Hz

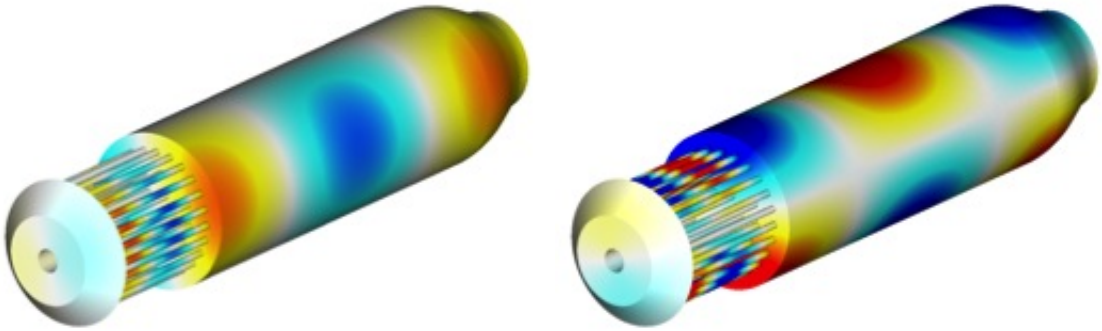

Fig. 7 Eigenmodes for case LP4.

References

[1] Poinsot, T., and Veynante, D., *Theoretical and numerical combustion*, R.T. Edwards, 2nd edition., 2005.

[2] Nicoud, F., Benoit, L., and Sensiau, C., "Acoustic Modes in Combustors with Complex Impedances and Multidimensional Active Flames," *AIAA Journal*, Vol. 45, 2007, pp. 426–441.

[3] Selle, L., Benoit, L., Poinsot, T., Nicoud, F., and Krebs, W., "Joint use of Compressible Large-Eddy Simulation and Helmoltz solvers for the analysis of rotating modes in an industrial swirled burner," *comb. flame*, Vol. 145, No. 1-2, 2006, pp. 194–205.

[4] DLR, "TEST CASE HF-7 - LOx/H2 Combustion with self-sustained acoustic excitation," Tech. rep., REST, 2013.

[5] Gröning, S., Hardi, J. S., Suslov, D., and Oschwald, M., "Injector-Driven Combustion Instabilities in a Hydrogen/Oxygen Rocket Combustor," *Journal of Propulsion and Power*, Vol. 32, No. 3, 2016, pp. 560–573. doi:10.2514/1.B35768, URL http://dx.doi.org/10.2514/1.B35768.

[6] Gröning, S., Hardi, J. S., Suslov, D., and Oschwald, M., "Influence of hydrogen temperature on the stability of a rocket engine combustor operated with hydrogen and oxygen," *CEAS Space Journal*, Vol. 9, No. 1, 2017, pp. 59–76. doi:10.1007/s12567-016-0130-8, URL http://dx.doi.org/10.1007/s12567-016-0130-8.